ORIGINAL ARTICLE

Cryogenic treatment analysis of electrodes in wire electric discharge machining of squeeze casted Al2024/Al$_2$O$_3$/W composite

Muhammad Huzaifa Raza[1] · Muhammad Asad Ali[2] · Waseem Tahir[3] · Ray Y. Zhong[1] · Nadeem Ahmad Mufti[2] · Naveed Ahmad[4]

Abstract

Peculiar characteristics of squeeze casted hybrid aluminum matrix composites (AMCs) enable it as an appropriate candidate for various manufacturing applications but also make their machining challenging. For that reason, wire electric discharge machining (WEDM) has been preferred over conventional machining processes for the cutting squeeze casted Al2024/Al$_2$O$_3$/W hybrid composite in this study. The presence of nanoparticles in the material affects the machining performance of wire electrodes. Therefore, molybdenum and zinc-coated wires have been chosen, and cryogenic treatment has been applied to improve their machining performance. To analyze the effects of cryogenic treatment, the machining efficiency of cryogenic treated (CT) wire has been compared with non-treated (NT) wire. Besides wire type, four key input variables including pulse duration (T_{ON}), wire feed rate (F_R), wire runoff speed (S_W), and wire tension (T_W) have also been optimized to improve the imperative response measures including cutting speed (CS), surface roughness (SR), and kerf width (KW). Microstructural analysis of NT wire depicts a high concentration of micro-voids, micro-cracks, and deep craters, while the surface of CT wire has been observed relatively fine after the machining. Comparative analysis of both wire electrodes has declared that CT wire yields 26.96% and 15.10% superior results for CS and SR respectively, and 6.92% deprived results for KW than NT wire. Grey relational analysis (GRA) has been practiced for multi-objective optimization and presented $T_{ON} = 3$ μs, $F_R = 13$ m/min, $S_W = 11$ m/min, and $T_W = 10$ g as an optimal set of input variables to achieve 75.1% and 72.5% overall results with NT and CT wire, respectively.

Keywords WEDM · Al2024/Al$_2$O$_3$/W · Squeeze casting · Cryogenic treatment

1 Introduction

In engineering materials, aluminum is the most alluring material due to its high strength, low weight, formability, recyclability, and corrosion resistance capability. Inadequate wear resistance and deprived performance at elevated temperatures are major concerns of aluminum alloys [1]. These deficiencies generally overcome by introducing reinforced particles in such alloys to produce aluminum matrix composites (AMCs) [2–5]. Reinforced particles in the metal matrix

✉ Muhammad Huzaifa Raza
huzaifa@connect.hku.hk

Muhammad Asad Ali
asad.ali@uet.edu.pk

Waseem Tahir
waseemtahirraja@gmail.com

Ray Y. Zhong
zhongzry@hku.hk

Nadeem Ahmad Mufti
namufti@uet.edu.pk

Naveed Ahmad
naveed527@gmail.com

1   Department of Industrial and Manufacturing Systems Engineering, The University of Hong Kong, 8/F, Haking Wong Building, Pok Fu Lam, Hong Kong

2   Department of Industrial and Manufacturing Engineering, University of Engineering and Technology, Lahore 54890, Pakistan

3   Department of Industrial Engineering, University of Engineering and Technology, Taxila 47080, Pakistan

4   Department of Industrial Engineering, College of Engineering and Architecture, Al-Yamamah University, Riyadh 11512, Saudi Arabia

improve the mechanical characteristics of AMCs by modifying the microstructural attributes. These superior properties of AMCs have enhanced their demand in marine, automotive, defense, and aerospace applications [6]. AMCs are generally fabricated by stir casting process, in which preheated reinforced particles are introduced in the matrix material and mixed uniformly with a mechanical stirrer [7]. Nevertheless, researchers have successfully boosted the mechanical properties of AMCs via the squeeze casting process [8].

Although the addition of reinforced particles improves the wear resistance and other mechanical properties of AMCs [9], the machining of such materials gets difficult by traditional means [10, 11]. Reinforcement in AMCs has abrasive nature and retains a drastic threat to the tool life. Abrasion during machining erodes the tool material at a faster rate and causes early failure of the tool [12]. Moreover, reinforced particles are pulled out during machining and act as an abrasive cutting edge which deteriorates the surface finish of work material [13, 14]. For this reason, wire electric discharge machining (WEDM) has been observed as a better substitute for the machining of AMCs because of no physical contact between tool and workpiece. In this machining process, electric sparks are generated between the electrode and workpiece and raise the interface temperature up to 12000 °C which eradicates the material by melting and evaporating [15, 16]. The electrode used in this machining is normally a thin wire of molybdenum, tungsten, brass, or copper having a diameter of 0.05–0.3 mm. Therefore, narrow kerfs (width of cut) are generated in the workpiece due to thin wire electrodes as compared to the conventional machining process which is also a perk of the WEDM process [17]. Dielectric fluid is generally used to maintain the insulating medium between electrode and workpiece. It also helps in flushing the eroded material from the machining zone due to high pressure [18]. Generally, the parts manufactured by composites or extremely hardened materials bearing intricate contours are machined precisely by the WEDM process with superior surface quality [19].

Keeping in view the demand in the manufacturing sector, researchers are focusing on the analysis of the working/machining behavior of hybrid AMCs due to their distinct properties. Therefore, several studies have been conducted to investigate the parametric effects on machining characteristics of various hybrid AMCs fabricated by different techniques. Muniappan et al. [20] described the effects of cutting parameters including V, I, T_{ON}, T_{OFF}, T_W, and F_R on the CS of Al6061/SiC/graphite hybrid AMC prepared by the stir casting process. T_{OFF} followed by T_{ON}, V, and I was observed as a significant parameter. Satishkumar and Kanthababu [21] compared the machined surface quality of simple Al7075 alloy and Al7075/B_4C/Al_2O_3 hybrid AMC fabricated by the stir casting process. It was noticed that simple Al7075 alloy at high T_{OFF} and low T_{ON} values generate comparatively less SR. Ugrasen et al. [22] investigated the influence of process

parameters (I, T_{ON}, T_{OFF}, and bed speed) on the machining of Al2024/TiC/fly-ash hybrid AMC synthesized by stir casting technique. At lower values of T_{OFF} and bed speed and higher values of I and T_{ON}, improved surface finish and dimensional accuracy were attained. Nag et al. [23] analyzed the impact of process parameters on the machining performance of A359/Al_2O_3/B_4C hybrid AMC produced by electromagnetic stir casting process. Analysis of the material removal rate and SR values showed T_{ON} as the most significant input variable. Kumar et al. [24] employed Al6351/SiC/B_4C hybrid AMC prepared by the stir casting technique for the parametric optimization in the WEDM process. Their findings revealed that concentration of boron carbide particles has a significant impact on SR. Prakash et al. [25] examined the influence of V, T_{ON}, T_{OFF}, F_R, and concentration of two distinct reinforced particles on material removal rate of Al356/B_4C/fly-ash hybrid AMC manufactured by the stir casting process. Their results declared that V and T_{ON} have considerable impact and concentration of reinforced particles has a negligible effect on material removal rate. Lal et al. [26] fabricated AA7075/SiC/Al_2O_3 hybrid AMC by inert gas-assisted electromagnetic stir casting technique to analyze the effects of input variables (T_{ON}, T_{OFF}, I, and S_W) on KW of AMC. From the literature, it has been observed that the machining performance of composites also depends upon the fabrication technique of the composite material [27]. Previous studies show that the machining of squeeze casted hybrid AMCs is scarcely reported.

To improve the machinability of hardened materials, cutting tools are treated cryogenically before machining. In cryogenic treatment, the material is kept at a very low temperature for a specific period resulting in improved electrical properties which are primarily imperative in electric discharge machining [28]. Superior electrical properties of electrodes yield high material removal rate and surface finish [29]. Besides this, tool life and wear resistance of the tools are also enhanced with appropriate cryogenic treatment [30]. In this type of treatment, cooling time, soaking rate, and temperature are the critical parameters that alter the properties of alloys [5, 31, 32]. Researchers have tried to optimize these parameters to achieve the desired material characteristics. Three particular sub-zero temperature ranges, (i) 223~193K (cold/cryogenic treatment), (ii) 193~113K (shallow cryogenic treatment), and (iii) 113~77K (deep cryogenic treatment), are mainly used for cryogenic treatment [33]. Tahir et al. [17] analyzed the effects of wire type (cold-treated brass wire and non-cold-treated brass wire) along with other input variables during machining HSLA steel. In wire type, cold-treated brass wire yielded better results as compared to non-cold treated brass wire. Kapoor et al. [34] employed shallow cryogenic treated and non-treated brass wire for the machining of EN-31 steel. Shallow cryogenic treated wire has significantly improved the machining due to improved electrical conductivity obtained as a result of

treatment. Kapoor et al. [35] compared the machining performance of non-cryogenic treated and deep cryogenic treated brass wire electrodes while cutting En-31 steel. Their results depict that deep cryogenic treatment of the brass wire resulted in better machining rate. Nayak and Mahapatra [36] used deep cryogenic treated wire (Bronco cut-W wire) and workpiece material (Inconel 718) to improve the machining performance evaluated by the results of angular error, SR, and CS. Goyal [29] investigated the effects of NT and CT wire in the machining of Inconel 625. On the basis of above discussed literature, it is observed that cryogenic treatment of electrode wire offered better results for CS and SR due to improve microstructure. Previous studies have presented the cryogenically treated electrodes as the best electrode alternative for the machining of hardened ferrous alloys, while machining of squeeze casted AMCs with cryogenically treated wire electrode is not adequately addressed in the literature.

From the comprehensive literature review, it has been reported that researchers have used AMCs prepared by various techniques in the WEDM process. However, there is a need to explore the machining of squeeze casted hybrid AMCs by the WEDM process. The compact packing of reinforcement particulates due to excessive squeeze pressure, machining of squeeze casted AMCs resulted in high electrode wear and SR [37]. Therefore, this research has been conducted to determine the appropriate wire electrode for the precise machining of the Al2024/Al$_2$O$_3$/W squeeze casted hybrid composite. As the material is squeeze casted, so it is also desired to identify the optimum set of input variables along with the selection of the best suitable wire type. For this reason, four input variables including pulse duration, wire tension, wire feed rate, and wire runoff speed have been used to analyze the effects of input variables on cutting speed, surface roughness, and kerf width. To investigate the appropriate wire type for the machining of Al2024/Al$_2$O$_3$/W, cryogenically treated moly wire, simple moly wire, cryogenic treated zinc-coated brass wire, and simple zinc-coated brass wire electrodes have been selected. Box-Behnken design of RSM has been adopted for experimental design, and ANOVA has been performed for analysis of the effects of input variables on response measures. For multi-objective optimization, grey relational analysis has been applied in this study.

2 Materials and methods

2.1 Fabrication of Al2024/Al$_2$O$_3$/W through squeeze casting technique

To analyze the effects of wire type and input variables on the machining performance of hybrid composite, Al2024/Al$_2$O$_3$/W has been fabricated by the squeeze casting process. The chemical composition of the matrix material used in the

preparation of hybrid AMC has been given in Table 1. For the desired assortment of mechanical properties of composite, Al$_2$O$_3$ (3wt%) and W (1.5 wt%) particles are used for the preparation of hybrid AMC having an average particle size of 10 nm and 200 nm respectively. Squeeze casting setup used for the preparation of hybrid AMC specimens has been displayed in Fig. 1.

The setup used for the fabrication of AMC comprised of an electric furnace for the preparation of melt and preheating of alumina and tungsten particles, a mechanical stirrer for the uniform blending of Al$_2$O$_3$ and W particles in the melt, a metallic die in which a mixture of Al$_2$O$_3$ and W particles and melt is poured, and a hydraulic press for squeezing the composite melt. Melting of substrate metal (Al2024) was carried out in the electric resistance furnace, and its superheat was maintained at 825 °C. To improve the wettability of Al$_2$O$_3$ and W particles in the metal matrix, particles were preheated at 950 °C for 3 h in the separate furnace. For the uniform distribution of Al$_2$O$_3$ and W particles in the metal matrix, a double stirring mechanism was opted. A prepared mixture of melt, Al$_2$O$_3$, and W particles was poured into the preheated (225 °C) metallic die and kept under high pressure of 100 MPa for 2 min. A solidified billet of hybrid AMC having 56-mm diameter and 140-mm height was extracted from the metallic die. For WEDM experimentation, 10-mm-thick slices were elicited from the cylindrical billet. The hardness of the specimens was determined by micro-Vickers hardness tester at a load of 0.5 kg for 20 s. The hardness of squeeze casted hybrid AMC was measured to be 165 HV. Due to the presence of nanoparticles and high squeeze pressure, the ultimate tensile strength (UTS) of fabricated hybrid AMC was also found exceptionally higher (441 MPa). To visualize the dispersion of nanoparticles throughout the metal matrix, SEM micrograph is shown in Fig. 2a. It can be seen that nanoparticles are distributed uniformly throughout the metal matrix; however, some clusters may exist due to high squeeze pressure. Microstructure of the composite material has also been analyzed at a higher resolution to visualize the dispersion of smaller sized Al$_2$O$_3$ particles (Fig. 2b).

2.2 Cryogenic treatment of wire electrodes

For the machining of the squeeze casted Al2024/Al$_2$O$_3$/W hybrid composite, two distinct wires including molybdenum and zinc-coated brass wires of diameter 0.3 mm have been selected. To enhance the electrical and mechanical properties,

Table 1 Chemical composition of matrix material (Al2024)

Elements	Ti	Si	Ni	Mg	Cu	Mn	Al
Wt%	0.02	0.15	0.03	1.21	3.84	0.60	Balanced

Reinforcement addition and stirring
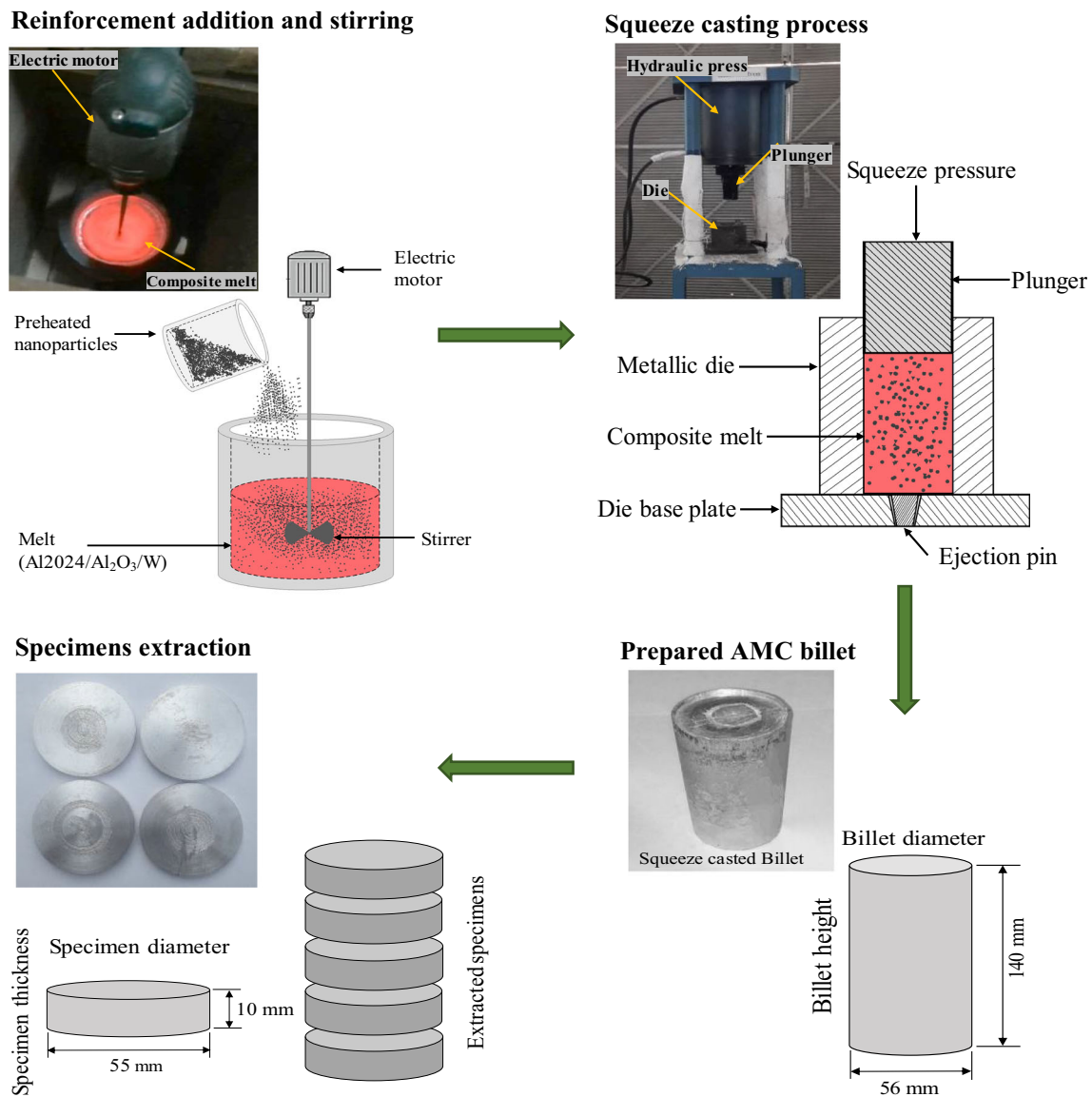
Squeeze casting process

Fig. 1 Hybrid AMC specimens' preparation through the squeeze casting process and its schematic illustration

selected wires have been cryogenically treated using a temperature-controlled electrical chamber (CTT-SC-7520-02FI). Soaking of both wires has been performed at -70 °C for 24h employing a ramp rate of 2 °C/min. After cryogenic treatment, electrical conductivities of treated and non-treated wires have been tested on a portable Kelvin Bridge tester.

Fig. 2 Microstructure of squeeze casted composite material showing **a** large-sized tungsten and **b** comparatively smaller sized Al_2O_3 nanoparticles shown at the higher resolution
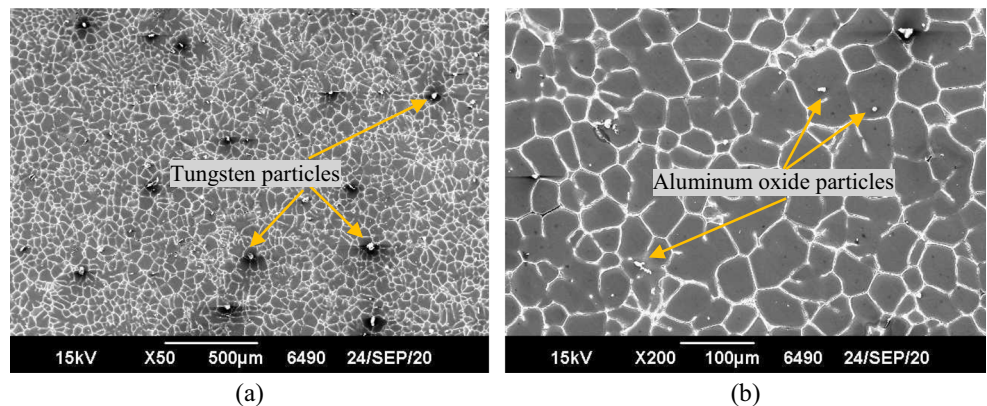
UTS of selected wires has been measured on a universal testing machine as per E8 ASTM standards. Results of electrical conductivity and UTS of tested wires are given in Table 2. It can be seen that UTS of molybdenum wire has increased to 1765 MPa while its electrical conductivity has been reduced from 2.08×10^7 to 2.02×10^7 S/m. In comparison with UTS, electrical conductivity is a fundamental property of the electrode for electric discharge machining. Reduced electrical conductivity of the electrode results in insufficient electrical spark density which affects the material removal process. This insufficient electrical conductivity declines CS and produces non-uniform and ineffective pulses which eventually generate poor surface finish [37]. Therefore, cryogenically treated molybdenum wire is seemed to be inappropriate for electric discharge machining hybrid AMC.

On the other hand, the UTS of zinc-coated brass wire has been slightly decreased from 727 to 686 MPa. It is due to the fact that the cryogenic treatment diminishes the residual stresses which are usually generated when material is formed into wires. Therefore, fracture toughness and wear properties increase, and UTS of the brass wire declines [38]. However, the electrical conductivity of cryogenic treated zinc-coated brass wire has been raised to 15.6×10^6 S/m with a percentage increment of 24.8%. Therefore, zinc-coated brass wires have been observed as an attractive option for machining. A framework has been developed for the selection of the best suitable wire electrode for the machining of the squeeze casted Al2024/Al$_2$O$_3$/W hybrid composite shown in Fig. 3. The machining performance of the wire electrode has been analyzed on the basis of CS, SR, and KW. Keeping wires' treatment results in view, cryogenic treated zinc-coated brass wire has been selected for the machining of composite material.

To have a deeper insight into the effects of cryogenic treatment, the microstructure of simple zinc-coated and cryogenic treated wires has been analyzed on a scanning electron microscope (SEM). The micrograph of NT wire reveals the presence of microcavities and pores in its structure (Fig. 4a). These microcavities offer hindrance in the flow of electrons which declines thermal and electrical conductivity. While the cryogenic treatment has increased the soundness and stability by reducing micro-cavities in its grain structure and can be seen in Fig. 4b. As temperature during the cryogenic treatment decreases, atomic bonding in brass starts to abate, and crystal structure regress towards its original phase. Residual stresses

in the brass wire structure are also minimized in cryogenic treatment [38]. Machining with CT wire depicts the intense electric discharge in the machining zone due to improved thermal and electrical conductivity as compared to NT wire. The same phenomenon of the machining of AMC with NT and CT wires is shown in Fig. 5a–b.

2.3 Experimentation details

To investigate the effects of wire type and input variables on the machining of hybrid AMC, a series of experiments has been conducted on WEDM. In wire type, cryogenic treated and simple zinc-coated brass wires have been selected for experimentation. Besides wire type, effects of input variables including pulse duration; wire tension; wire feed rate; and wire runoff speed on cutting speed, surface roughness, and kerf width have also been analyzed. Pilot experimentation has been conducted to explore the appropriate ranges of input variables for machining of Al2024/Al$_2$O$_3$/W hybrid composite. Selected ranges of input variables have been given in Table 3. Machining conditions other than input variables are provided in Table 4. For each experiment, CS has been determined by recording the cutting time of a predetermined cutting length of 27 mm. CS values obtained from the control unit of the machine have been used to verify the calculated values of CS. SR of the cutting specimens has been measured using surface roughness tester (SJ-410). A coordinate measuring machine (CE-450DV) of 0.001-mm resolution has been employed for the measurement of KW. Surface morphology of wire and machined surfaces of workpiece has been analyzed on SEM (VEGA3) facility. The methodology of this research starting from machining to response measurement is shown in Fig. 6.

2.4 Experimental design

2.4.1 Response surface methodology

In previous studies, numerous statistical techniques including factorial design [39], Taguchi method [40], response surface methodology [41], genetic algorithm [42], fuzzy logic [43], and artificial neural network [44] have been practiced for the design of experiments, analysis, empirical modeling, and optimization. In all types of designed experiments, there exist some variations in experimental results. However, RSM

Table 2 Effect of cryogenic treatment on electrodes' properties

| Wire type	Electrical conductivity (S/m)	UTS (MPa)
Simple molybdenum wire	2.08×10^7	1652
Cryogenic treated molybdenum wire	2.02×10^7	1765
Zinc-coated brass wire	12.5×10^6	727
Cryogenic treated zinc-coated brass wire	15.6×10^6	686

Fig. 3 Framework for the selection of appropriate wire electrode for the machining of the squeeze casted Al2024/Al$_2$O$_3$/W hybrid composite

repeats some basic experiments known as center point experiments to minimize these variations. Replication of experiments enables the researcher to identify and reduce the

experimental error. It also increases the accuracy and presents a more precise estimation of response variables in mathematical modeling. Moreover, RSM has distinctive capabilities of

Fig. 4 Microstructure of **a** non-treated and **b** cryogenically treated brass wire
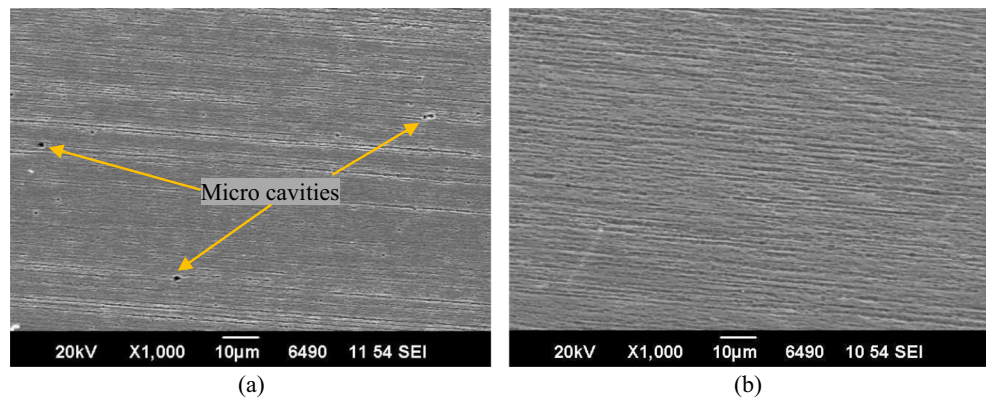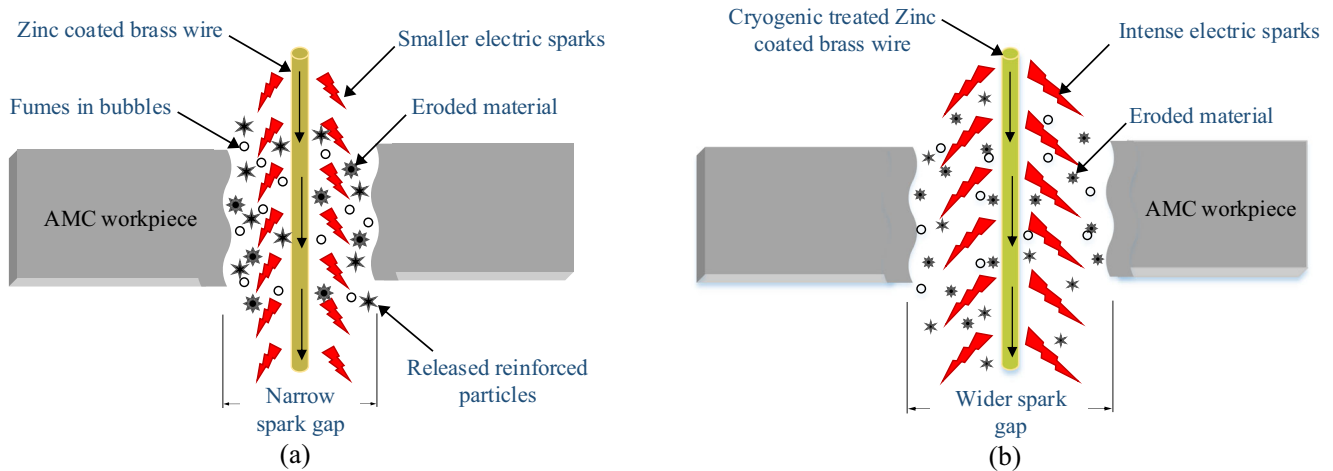
Fig. 5 Schematic illustration of the machining of AMC with **a** simple zinc-coated brass wire and **b** cryogenic treated zinc-coated brass wire

generating a reduced number of experiments for the development of empirical models with great accuracy; hence, RSM is regarded as the most effective approach for analysis [45].

Box-Behnken design of RSM has been used for the design of experiments in this study. The design offers 30 experiments with 4 input variables at 3 distinct levels. The complete design has been repeated for both cryogenic treated and simple zinc-coated brass wires separately; therefore, a total of 60 experiments have been conducted in this research. Results of CS, SR, and KW against each set of input variables for both wires are given in Table 5.

3 Results and discussions

This section covers the analysis of response measures by ANOVA, empirical modeling of individual response measures, analysis of the effects of input variables using 3D response surface graphs, microstructural analysis, multi-objective optimization using GRA, and performance comparison of NT and CT wire electrodes.

3.1 Main and interaction effects analysis

The effects of input variables on the response measures are presented in the form of 3D response surface graphs. The 3D surface of the graph depicts the main as well as the interaction effects of two input variables simultaneously while keeping other variables constant at their mid-levels [46]. Contour lines on the base of the graph depict the reflection of 3D surface. Contour lines with distinct colors present the range of response values from minimum to maximum.

3.1.1 Cutting speed

The effects of F_R, T_{ON}, T_W, and S_W on the CS for both NT and CT wires are shown in Fig. 7a–d. It has been observed that CS increases with an increment in both T_{ON} and F_R (Fig. 7a–b). The value of CS is smaller at the lower level of T_{ON} as discharge energy is provided for a shorter time span which enables the reinforced particles to protect the metal matrix from melting with their strong bonding with matrix. With an increase in T_{ON}, the discharge energy is supplied for more time to eradicate material from the work surface. This intense discharge energy melts and evaporates aluminum matrix easily and releases the reinforced particles; this is the reason that a slight increase in T_{ON} raises the CS promptly. Similar trends of T_{ON} have been reported by Kavimani et al. [47]. High CS has been observed at a higher level of F_R. Increase in F_R value raises the chance of new wire to expose and create clear and higher intensity sparks. This intense spark energy is responsible for material erosion by broadening and deepening the cutting zone [48].

Table 3 Description of input variables and their selected ranges

Input variables	Description	Ranges
Pulse duration	The time interval in which discharge is produced	1–5 μs
Wire feed rate	The rate at which wire passes through the guided path in a transverse direction	10–16 m/min
Wire runoff speed	Wire velocity along its longitudinal direction	5–11 m/min
Wire tension	Mechanical stress maintained in the wire	4–10 g

Table 4 Constant machining conditions

Machining conditions	Description
Gap voltage	45 V
Pulse off time	26 μs
Servo voltage	48 V
Flushing pressure (kg/cm^2)	4.5
Dielectric fluid	Water mixed resin MBQR400 (ratio 30:1)

Figure 7c–d show the effects of S_W and T_W on CS. It has been noticed that CS enhances by an increase in S_W with a nonlinear trend. An increment in S_W increases the rate of spark discharge which leads to the high amount of heat energy delivered to the cutting zone that ultimately enhances the rate of melting and evaporation of work material [49]. From Fig. 7c–d, it has been observed that the increase in T_W improves the CS of composite material due to increased straightness of wire, while low CS has been reported at lower T_W because wire vibrates and lags behind during cutting [50]. Within the suitable range of T_W, CS increases with T_W.

Comparatively analysis of the performance of both wire electrodes in Fig. 7 shows that CS of CT wire is high during the cutting of squeeze casted hybrid AMC. As in cryogenic treatment, the crystal structure of the electrode gets refines and makes the electron flow uniform and easier. The absence of any obstacle in the structure of electrode material enhances the electron flow per unit time which improves the electrical conductivity of the cryogenically treated material. Owing to the high electrical conductivity of cryogenically treated brass

wire, a high amount of energy is supplied to the machining zone which melts and evaporates matrix material at a faster rate. Intense sparking is produced which removes more material from the machining zone, and the same phenomenon can be observed in Fig. 4b. It releases the reinforced particles from the matrix swiftly which increases the material removal rate and ultimately enhances the CS.

3.1.2 Surface roughness

The 3D response graphs for NT and CT wires presenting the effects of input variables on SR are shown in Fig. 8a–d. It is cleared from Fig. 8a–b that SR is maximum at a higher level of T_{ON} and F_R. Increase in feed rate, the wire gets renewed and recovered hastily during machining. This introduction of non-worn fresh wire apparently enhances the sparking efficiency which creates larger and deeper craters [48]. While an increase in T_{ON} increases the time duration for the electric sparks which melts more workpiece material and produces large-sized craters. These large-sized craters create irregularities on the machined surface eventually increase the SR [51].

Figure 8c–d depict the effects of S_W and T_W on SR for both NT and CT wires respectively. It has been observed that SR rises initially and then starts decreasing with the further increase in S_W. Increase in S_W allows the molten material to splash on the work surface with the flushing pressure, and micro-voids are created due to the entrapment of gases. As a result of micro-voids in the molten pool, high SR is originated [52]. On the other hand, SR declines with an increase in T_W which is actually due to the decrease in wire amplitude at
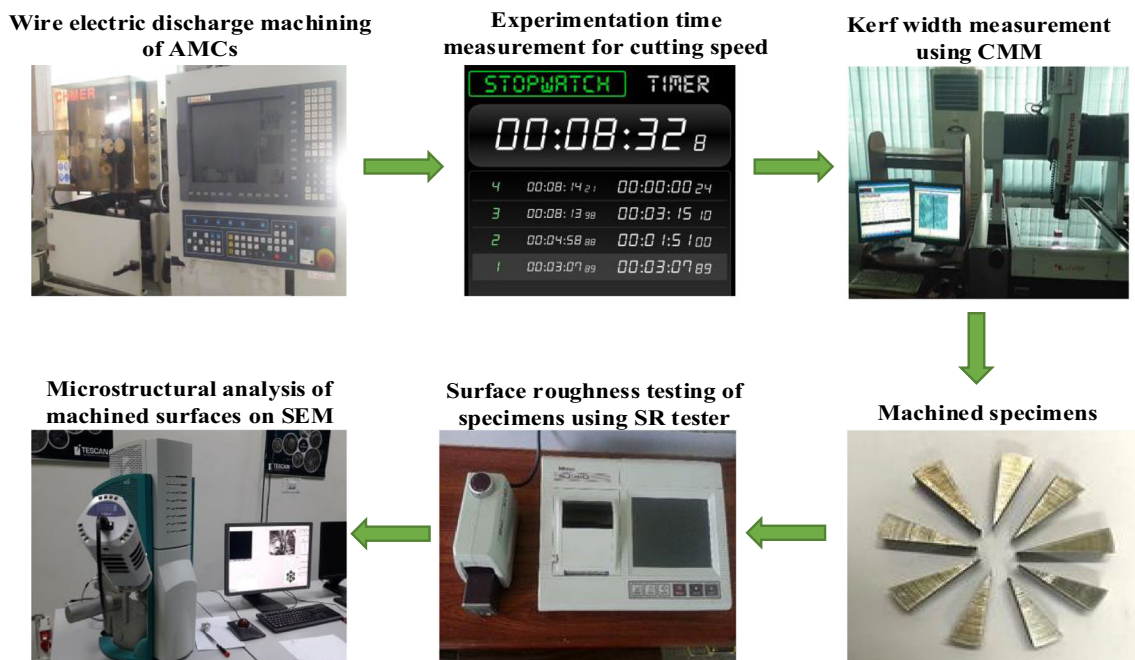

Fig. 6 Experimental procedure and response measurement

Table 5 Design matrix with measured response values

Exp. no.	Input variables				Response measures					
	Pulse duration (T_{ON})	Wire feed rate (F_R)	Wire runoff speed (S_W)	Wire tension (T_W)	Zinc-coated brass wire			Cryogenic treated zinc-coated brass wire		
					Cutting speed mm/min	Surface roughness μm	Kerf width mm	Cutting speed mm/min	Surface roughness μm	Kerf width mm
	μs	m/min	m/min	g						
1	1	10	8	7	1.88	2.35	0.401	2.05	1.95	0.443
2	5	10	8	7	5.13	3.01	0.429	6.21	2.57	0.471
3	1	16	8	7	3.07	2.59	0.349	3.67	2.21	0.354
4	5	16	8	7	7.16	3.84	0.409	9.09	3.12	0.440
5	3	13	5	4	2.30	2.39	0.398	2.73	1.98	0.437
6	3	13	11	4	3.16	2.75	0.384	3.74	2.09	0.421
7	3	13	5	10	2.92	2.29	0.368	3.13	1.42	0.405
8	3	13	11	10	3.83	2.15	0.318	5.37	1.82	0.340
9	1	13	8	4	1.84	2.19	0.395	1.86	1.84	0.425
10	5	13	8	4	5.15	3.48	0.422	5.93	2.98	0.439
11	1	13	8	10	2.20	2.23	0.342	2.35	1.89	0.355
12	5	13	8	10	6.05	2.91	0.399	7.53	2.33	0.429
13	3	10	5	7	2.82	1.92	0.405	3.60	1.63	0.447
14	3	16	5	7	4.40	2.34	0.377	5.72	2.02	0.413
15	3	10	11	7	3.65	2.10	0.387	4.67	1.81	0.426
16	3	16	11	7	5.15	2.72	0.358	6.68	2.33	0.391
17	1	13	5	7	1.76	2.01	0.393	1.94	1.57	0.433
18	5	13	5	7	4.89	2.93	0.430	5.94	2.36	0.472
19	1	13	11	7	2.32	2.19	0.374	2.67	1.73	0.412
20	5	13	11	7	6.37	3.19	0.409	7.84	2.59	0.451
21	3	10	8	4	2.41	2.31	0.408	2.73	1.99	0.459
22	3	16	8	4	3.97	3.00	0.376	4.82	2.58	0.397
23	3	10	8	10	2.98	2.17	0.372	3.46	1.85	0.388
24	3	16	8	10	4.71	2.71	0.346	5.76	2.33	0.377
25	3	13	8	7	3.68	2.38	0.376	4.05	1.89	0.404
26	3	13	8	7	3.92	2.31	0.379	4.30	1.83	0.407
27	3	13	8	7	3.57	2.46	0.382	3.84	1.96	0.412
28	3	13	8	7	3.65	2.38	0.375	4.14	1.89	0.403
29	3	13	8	7	3.74	2.51	0.371	4.22	1.92	0.398
30	3	13	8	7	3.61	2.47	0.388	4.06	1.97	0.417

higher tension. Due to high T_W, the wire gets straightened, and fluid begins to flow with higher speed around the wire which prevents the debris from adherence and keeps the workpiece surface clean. This ablution of the surface is responsible for low SR at higher T_W [50].

From response surface graphs in Fig. 8, it has been observed that CT wire yields less SR as compared to NT wire. Earlier discussion on cryogenic treatment shows that CT wire has high electrical conductivity, which is also responsible for the reduction in SR. Because higher electrical conductivity of the electrode widens the electric discharge channel which results in easier flushing of debris and discards reinforced

particles from the machining zone and keeps the machined surface smooth and clean. Moreover, this enlarged discharged channel distributes the spark energy uniformly in all orientations which produces small and uniform sized craters on the machined surface as compared to NT wire, and the same behavior of CT wire can be realized in Fig. 5a–b. Therefore, CT wire results in superior surface quality for composite material.

3.1.3 Kerf width

KW is the gap created as a result of the cutting process that increases or decreases with variation in machining parameters.
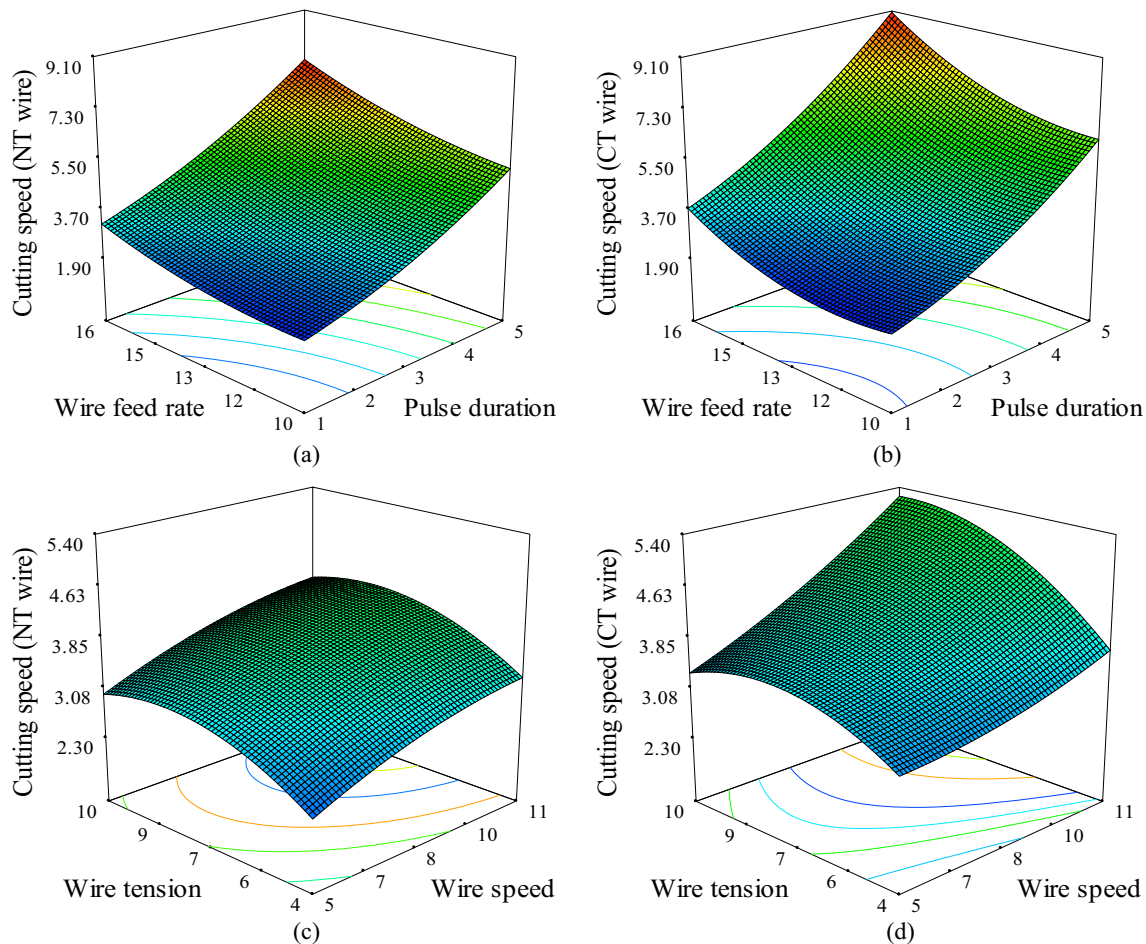
Fig. 7 The 3D response surface graphs presenting the effects of T_{ON} and F_R on CS for **a** NT wire and **b** CT wire and S_W and T_W on CS for **c** NT wire and **d** CT wire

Changes in KW with variation in input variables are presented in Fig. 9a–d. In this study, it has been observed that KW of hybrid AMC reduces with the decrease in F_R and increase in Ton (Fig. 9a–b). However, T_{ON} has a significant impact on KW as compared to F_R, as the increase in T_{ON} offers more time to discharge energy for melting and vaporizing the work material. At a low level of T_{ON}, discharge energy is not sufficient to remove work material easily, while at higher values of T_{ON}, intense discharge energy melts the substrate metal and breaks the Al_2O_3 and W particles bound from the matrix. Thus, removal of reinforcement particles increases the KW significantly. It has been observed that an increase in F_R decreases the KW because a higher feed rate does not let the wire electrode to distribute heat energy uniformly in the cutting zone. Therefore, the ineffective distribution of heat energy in the machining zone results in reduced KW.

From Fig. 9c–d, it can be clearly seen that KW is minimum at higher values of T_W and S_W. When S_W is low, the amplitude of wire vibration is comparatively higher which reduces the dielectric fluid flow around the wire and resulted in inefficient eradication of debris and reinforced particles from the discharge gap. Moreover, the debris particles

which adhered around the wire also generate high KW. When the wire is running at a higher speed, the debris and reinforced particles get discarded from the wire surface and resulted in reduced KW [53]. From the 3D surface graph, it can be seen that KW decreases as tension in the wire increases. At low T_W, the amplitude of the wire is comparatively high resulted in a wider kerf. Average vibration amplitude decreases with an increase in T_W which ultimately yields narrow KW [54].

From Fig. 9, it has been observed that CT wire generated wider kerf than NT wire in AMC. This increase in kerf is due to the higher electrical conductivity of CT wire. The high electrical conductivity of the electrode produces intense discharge energy to the machining zone and removes a high amount of composite material. Improved flushing using CT wire prevents debris and residue material from adherence and keeps the spark gap cleaner. Moreover, the melting of matrix material releases the large-sized reinforced particles from the machining zone which also increases the spark gap abruptly. The actual phenomenon of the widening of spark gap is illustrated in Fig. 5 schematically. This increase in spark gap resulted in high kerf width of composite material with CT wire.
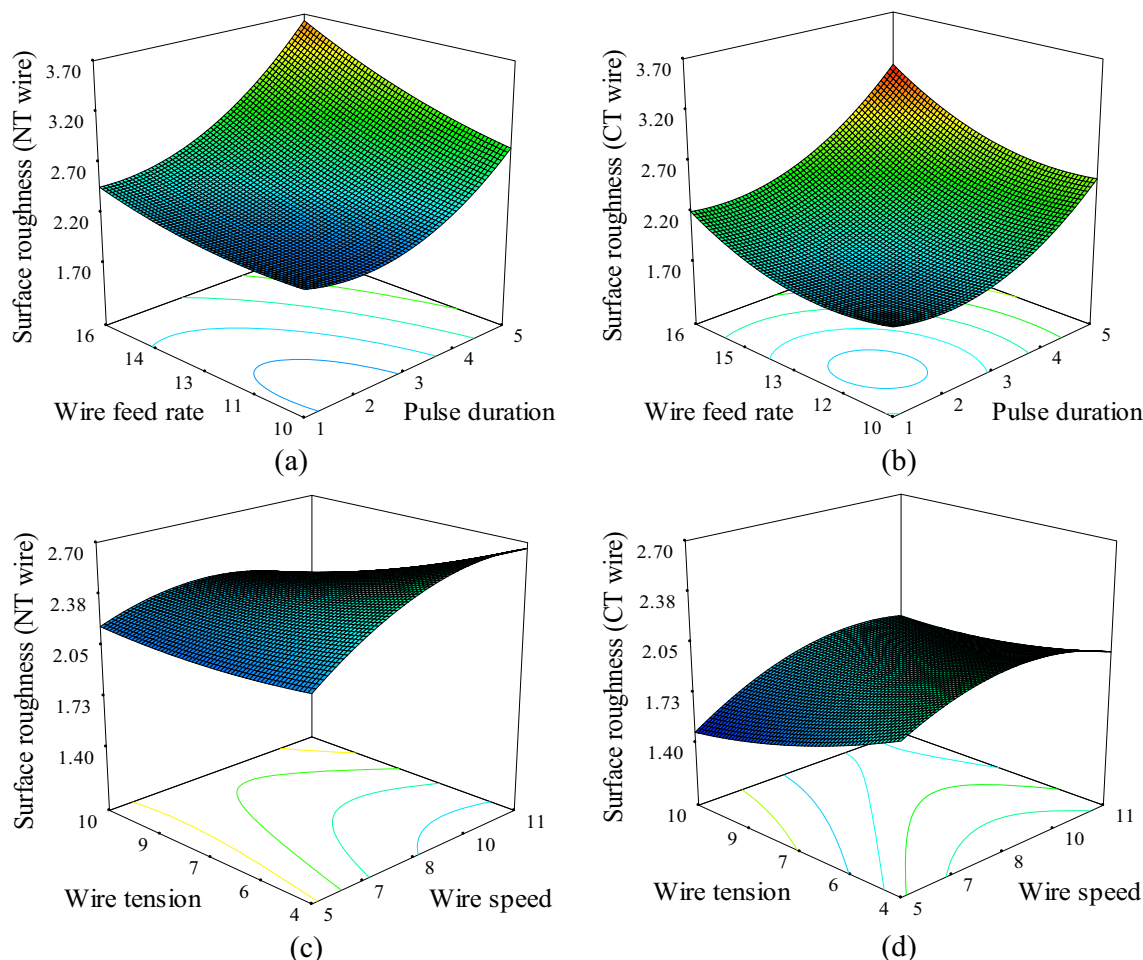
Fig. 8 The 3D response surface graph for the effects of T_{ON} and F_R on SR for **a** NT wire and **b** CT wire and S_W and T_W on SR for **c** NT wire and **d** CT wire

3.2 Microstructural analysis

3.2.1 Surface morphology of workpiece

Material characteristics highly depend upon the microstructure and grain growth upon solidification of the material [55]. The surface morphology of the machined specimens has been analyzed using SEM shown in Fig. 10a–d. To clearly visualize the effects of input variables and cryogenic treatment of the wire electrode, the surface morphology of specimens machined with NT and CT wires has been compared. For this aspiration, specimens bearing minimum and maximum SR values are analyzed at exp. nos. 13 and 04, respectively, which are provided in Table 5 for both wire electrodes. Better surface morphologies of NT (1.92 μm) and CT wire (1.63 μm) have been seen at T_{ON} = 3 μs, F_R = 10 m/min, S_W = 5 m/min, and T_W = 7 g displayed in Fig. 10a–b respectively. On the other side, Fig. 10c–d display deprived surfaces of machined specimens (3.84 μm and 3.12 μm for NT and CT wire respectively) at T_{ON} = 5 μs, F_R = 16 m/min, S_W = 8 m/min, and T_W = 7 g. From the above comparison, it has been seen that NT wire

results in inferior surface morphology than CT wire in both cases. Surface morphology of specimens machined with NT wire depicts micro-voids, globules, and large craters, while CT wire resulted in small and shallow sized craters, and few debris particles welded on the surface have also been noticed. The reason behind the remarkable performance of CT wire is the enlarged discharge channel which prevents the melted material from re-solidification on the work surface and makes the flushing easy due to its superior electrical conductivity.

3.2.2 Kerf width

To visualize the difference in the performance of NT and CT wire electrodes, micrographs at lower and higher values of KW have been compared. For this purpose, the KW of both wires has been analyzed at exp. nos. 08 and 18 showing the minimum and maximum values which are presented in Table 5. From Fig. 11a–b, it can be observed that low energy parameters (T_{ON} = 3 μs, F_R = 13 m/min, S_W = 11 m/min, and T_W = 10 g) at exp. no. 08 has generated narrow kerf. When the comparison has been made between Fig. 11 a and b, it can be
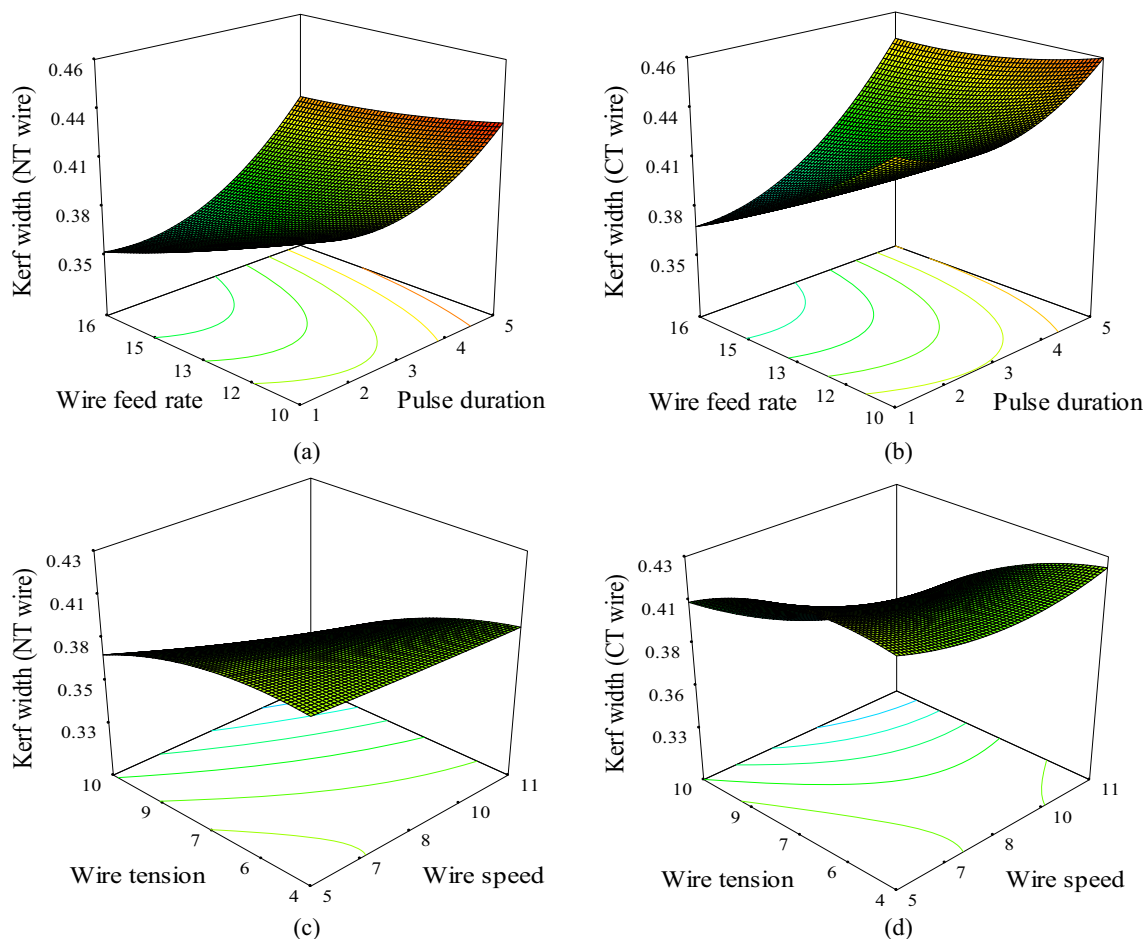
Fig. 9 3D response surface graph showing the influence of T_{ON} and F_R on KW for **a** NT wire and **b** CT wire and S_W and T_W on KW for **c** NT wire and **d** CT wire

seen that CT wire has produced a relatively higher KW value (0.340 mm) than NT wire (0.318 mm). However, high energy parameters $T_{ON} = 5$ μs, $F_R = 13$ m/min, $S_W = 5$ m/min, and $T_W = 7$ g at exp. no. 18 have resulted in wider kerfs 0.430 mm and 0.472 mm for NT and CT wires respectively. High energy parameters result in high explosions and intense sparking which ultimately produce large-sized kerf. In comparison with CT wire, NT wire has produced narrow KW due to poor flushing and allows the debris material to re-solidify on the machined surface, and the same phenomenon can be observed in Fig. 11c–d.

3.2.3 Wire surface analysis

In the machining of squeeze casted hybrid composite, the effects of wire's cryogenic treatment and machining variables have also been analyzed on wire surface. For this mean, micrographs of NT and CT wire have been compared at exp. no. 04. In Fig. 12, the surface integrity of both wires shows the difference in erosion patterns during the machining of squeeze casted hybrid composite. Micrograph of eroded NT wire in Fig. 12a depicts some micro-cracks and clusters of voids on its

surface. Besides this, larger and deeper craters have also been observed on their surface after machining. On the other hand, a shallow and small-sized crater has been seen on the CT wire's surface (Fig. 12b). At the same cutting conditions (exp. no. 04), wear performance of wires shows that NT wire degenerates more swiftly as compared to CT. During machining, high temperature in the machining zone decreases the thermal conductivity of the wire electrode which melts and evaporates wire material and deteriorates the wire structure. Depreciation in wear behavior of CT wire is certainly due to the enhanced thermal and electrical conductivity attained during cryogenic treatment which ultimately results in a comparatively smooth wire surface [56].

3.3 Analysis of variance

To analyze the effects of input variables, the design of experiment has been formulated using a statistical technique. Each technique involves randomization as a basic principle in experimental design. These techniques randomly allocate the experimental units as well as conduct experiments randomly. This randomization avoids biases in the conclusions for input

Fig. 10 Microstructure of the machined surfaces at exp. no. 13 for **a** NT and **b** CT wires and exp. no. 04 for **c** NT and **d** CT wires
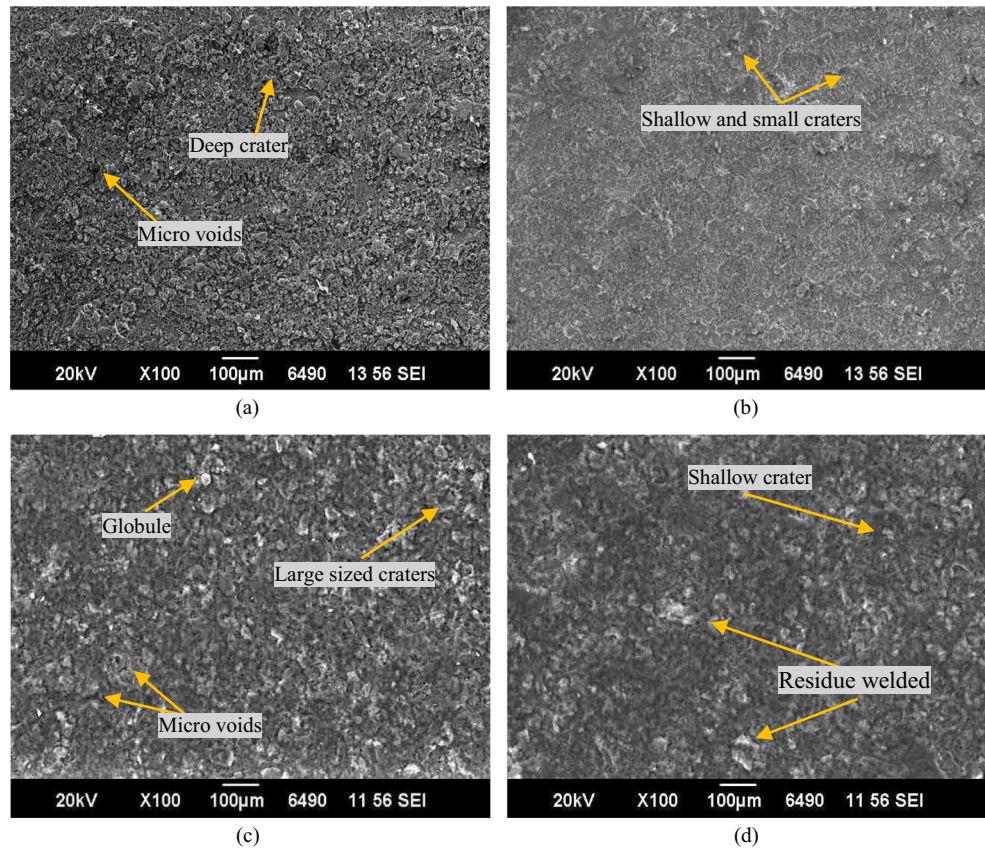
variables. After designing the experiment, results are analyzed with analysis of variance (ANOVA). ANOVA distributes the total variation into accountable sources of variations (input variables) in the experiments [57]. ANOVA also estimates the percentage contribution of input variables and their interactions into the corresponding response measures. To predict the response measures, empirical models for each response measure have been developed using experimental results. Statistical significance of developed empirical models, main, interaction, and quadratic terms has also been assessed in this study [58]. The coefficient of determination (R^2) ascertains the linear correlation of variables and response measures in the regression analysis, and its higher values depict the adequacy of developed empirical models [59]. An adequate

empirical model has the ability to predict the response measures with great accuracy.

3.3.1 Cutting speed

ANOVA of the CS results for both NT and CT wire electrodes has been provided in Table 6. Fit summary shows that all input variables have a significant impact on CS for both electrodes using 95% confidence level. The analysis shows that empirical models of CS for both wire electrodes are significant and adequacy measures (R^2, adjusted R^2, and predicted R^2) are also in reasonable agreement. This reveals that developed models for CS can predict response values with fine accuracy. Developed empirical models for NT and CT wires are presented in Eqs. (1) and (2) respectively:

$$
\begin{aligned}
\text{Cutting speed (NT wire)} =\ & 1.965 - 0.575 \times T_{ON} - 0.762 \times F_R + 0.336 \times S_w + 0.611 \times T_W + (0.034 \times T_{ON} \times F_R) \\
& + (0.038 \times T_{ON} \times S_w) + (0.022 \times T_{ON} \times T_W) - (2.50 \times 10^{-3} \times F_R \times S_w) \\
& + (4.75 \times 10^{-3} \times F_R \times T_W) + (1.25 \times S_w \times T_W) + (0.093 \times T_{ON}^2) \\
& + (0.035 \times F_R^2) - (0.017 \times Ç S_w) - (0.045 \times T_W^2)
\end{aligned}
\tag{1}
$$

Fig. 11 Micrograph showing minimum KW values at exp. no. 08 using **a** NT wire and **b** CT wire and maximum KW values at exp. no. 18 with **c** NT wire and **d** CT wire

(a)

(b)

(c)

(d)
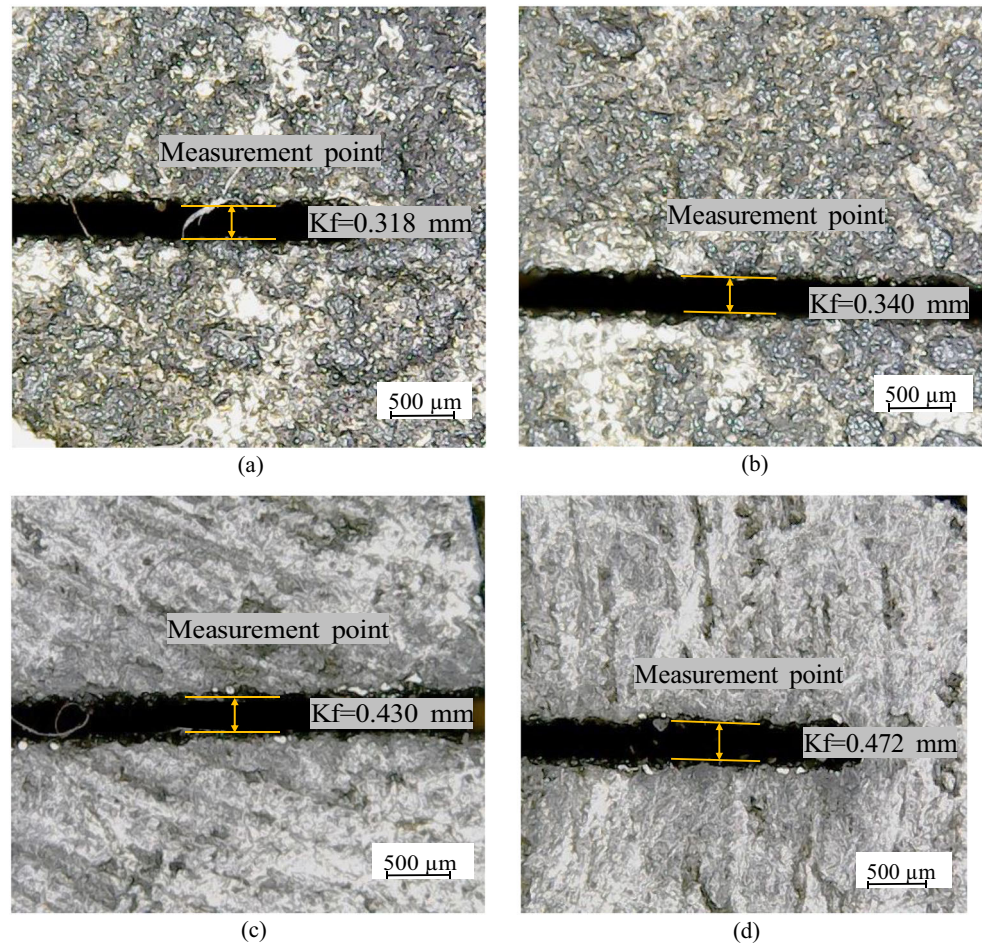
$$
\begin{aligned}
\text{Cutting speed (CT wire)} = {}& 12.204 - 1.019 \times T_{ON} - 1.819 \times F_R + 0.375 \times S_w + 0.348 \times T_W + (0.052 \times T_{ON} \times F_R) \\
& + (0.048 \times T_{ON} \times S_w) + (0.046 \times T_{ON} \times T_W) - (3.19 \times 10^{-3} \times F_R \times S_w) \\
& + (6.06 \times 10^{-3} \times F_R \times T_W) + (0.034 \times S_w \times T_W) + (0.130 \times T_{ON}^2) \\
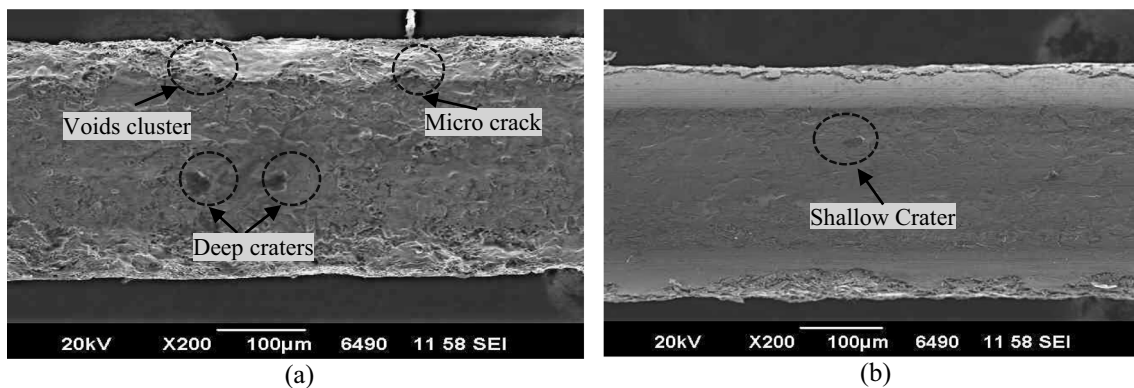& + (0.077 \times F_R^2) - (0.015 \times S_w^2) - (0.048 \times T_W^2)
\end{aligned} \tag{2}
$$

(a)

(b)

Fig. 12 Microstructure of **a** NT and **b** CT wire after experimentation

Table 6 Analysis of variance showing p-values of CS, SR, and KW for NT and CT wires

Source	Cutting speed		Surface roughness		Kerf width		
	NT wire	CT wire	NT wire	CT wire	NT wire	CT wire	
Model	< 0.0001	< 0.0001	< 0.0001	< 0.0001	< 0.0001	< 0.0001	Significant
T_{ON}	< 0.0001	< 0.0001	< 0.0001	< 0.0001	< 0.0001	< 0.0001	
F_R	< 0.0001	< 0.0001	< 0.0001	< 0.0001	< 0.0001	< 0.0001	
S_W	< 0.0001	< 0.0001	0.0068	< 0.0001	< 0.0001	0.0004	
T_W	< 0.0001	< 0.0001	0.0007	< 0.0001	< 0.0001	< 0.0001	
$T_{ON} \times F_R$	0.0208	0.0304	0.0212	0.0338	0.0274	0.0144	
$T_{ON} \times S_W$	0.0126	0.0432	0.7513	0.6087	0.8807	0.9925	
$T_{ON} \times T_W$	0.1189	0.0536	0.0197	< 0.0001	0.0369	0.0126	
$F_R \times S_W$	0.7850	0.8315	0.3901	0.2871	0.9401	0.9623	
$F_R \times T_W$	0.6054	0.6867	0.5213	0.3430	0.6534	0.0276	
$S_W \times T_W$	0.8914	0.0339	0.0440	0.0290	0.0149	0.0309	
T_{ON}^2	< 0.0001	0.0001	< 0.0001	< 0.0001	< 0.0001	0.0002	
F_R^2	0.0001	< 0.0001	0.0359	< 0.0001	0.3333	0.2383	
S_W^2	0.0234	0.1876	0.0022	< 0.0001	0.8442	0.0225	
T_W^2	< 0.0001	0.0006	0.3863	0.0246	0.0036	0.0088	
Lack of fit	0.2095	0.0833	0.1066	0.2847	0.4030	0.1006	Insignificant
Model summary							
R^2	0.993	0.989	0.966	0.988	0.967	0.947	
$R^2_{Adjusted}$	0.986	0.979	0.933	0.976	0.935	0.898	
$R^2_{Predicted}$	0.965	0.943	0.822	0.942	0.847	0.725	
Adq. precision	48.322	39.432	21.575	39.346	21.848	16.438	

3.3.2 Surface roughness

ANOVA results in Table 6 explain that empirical models of SR for NT and CT wire electrodes are significant as their probability values are less than 0.05 [60]. It is also observed that all input variables have also a significant effect on SR.

Adequacy measures have also been focused during the analysis to check the adequacy of empirical models. Numerical values of all coefficients are closer to 1 which shows the competitive prediction capabilities of developed SR models for both wires which are presented in Eqs. (3) and (4):

$$
\begin{aligned}
\text{Surface roughness (NT wire)} = {}& 2.168 - 0.425 \times T_{ON} - 0.285 \times F_R + 0.334 \times S_w + 0.132 \times T_W + (0.024 \times T_{ON} \times F_R) \\
& + \left(3.06 \times 10^{-3} \times T_{ON} \times S_w\right) - (0.024 \times T_{ON} \times T_W) \\
& + \left(5.59 \times 10^{-3} \times F_R \times S_w\right) - \left(4.15 \times 10^{-3} \times F_R \times T_W\right) - (0.013 \times S_w \times T_W) \\
& + \left(0.083 \times T_{ON}^2\right) + \left(0.011 \times F_R^2\right) - \left(0.017 \times S_w^2\right) + \left(4.31 \times 10^{-3} \times T_W^2\right)
\end{aligned}
\tag{3}
$$

$$
\begin{aligned}
\text{Surface roughness (CT wire)} = {}& 4.789 - 0.241 \times T_{ON} - 0.598 \times F_R + 0.213 \times S_w - 0.074 \times T_W + (0.011 \times T_{ON} \times F_R) \\
& + \left(2.62 \times 10^{-3} \times T_{ON} \times S_w\right) - (0.029 \times T_{ON} \times T_W) \\
& + \left(3.69 \times 10^{-3} \times F_R \times S_w\right) - \left(3.27 \times 10^{-3} \times F_R \times T_W\right) + \left(8.07 \times 10^{-3} \times S_w \times T_W\right) \\
& + \left(0.078 \times T_{ON}^2\right) + \left(0.024 \times F_R^2\right) - \left(0.018 \times S_w^2\right) + \left(6.38 \times 10^{-3} \times T_W^2\right)
\end{aligned}
\tag{4}
$$

3.3.3 Kerf width

ANOVA of KW results for NT and CT wires has also been presented in Table 6. From the analysis, it has been observed that the probability values of models are lower than 0.05 which guarantees the significance of developed models.

Input variables including T_{ON}, F_R, S_W, and T_W have a significant contribution in KW produced by NT and CT wires. Reasonable values of adequacy measures show the proficiency of developed models. Developed empirical models of KW for both NT and CT wire are given in Eqs. (5) and (6) respectively:

$$
\begin{aligned}
\text{Kerf width (NT wire)} = {} & 0.572 - 0.044 \times T_{ON} - 0.017 \times F_R + 2.80 \times 10^{-3} \times S_w - 8.88 \times 10^{-3} \times T_W \\
& + \left(1.33 \times 10^{-3} \times T_{ON} \times F_R\right) - \left(8.33 \times 10^{-5} \times T_{ON} \times S_w\right) \\
& + \left(1.25 \times 10^{-3} \times T_{ON} \times T_W\right) - \left(2.77 \times 10^{-5} \times F_R \times S_w\right) \\
& + \left(1.66 \times 10^{-4} \times F_R \times T_W\right) - \left(1.0 \times 10^{-3} \times S_w \times T_W\right) + \left(4.84 \times 10^{-3} \times T_{ON}^{\varsigma}\right) \\
& + \left(2.77 \times 10^{-4} \times F_R^2\right) + \left(5.55 \times 10^{-5} \times S_w^2\right) - \left(9.58 \times 10^{-4} \times T_W^2\right)
\end{aligned}
\tag{5}
$$

$$
\begin{aligned}
\text{Kerf width (CT wire)} = {} & 0.894 - 0.066 \times T_{ON} - 0.038 \times F_R - 0.012 \times S_w - 3.96 \times 10^{-3} \times T_W \\
& + \left(2.40 \times 10^{-3} \times T_{ON} \times F_R\right) - \left(8.33 \times 10^{-6} \times T_{ON} \times S_w\right) \\
& + \left(2.45 \times 10^{-3} \times T_{ON} \times T_W\right) - \left(2.77 \times 10^{-5} \times F_R \times S_w\right) \\
& + \left(1.41 \times 10^{-3} \times F_R \times T_W\right) - \left(1.37 \times 10^{-3} \times S_w \times T_W\right) + \left(4.91 \times 10^{-3} \times T_{ON}^2\right) \\
& + \left(5.42 \times 10^{-4} \times F_R^2\right) + \left(1.12 \times 10^{-3} \times S_w^2\right) - \left(1.32 \times 10^{-3} \times T_W^2\right)
\end{aligned}
\tag{6}
$$

3.4 Multi-objective optimization

WEDM is a susceptible and delicate machining technique that requires intensive surveillance because of its sensitivity toward numerous electrical and non-electrical control parameters. Slight variation in a parameter may result in a convoluted impact on response measure. Therefore, it is inevitable to perform machining without an optimum set of input variables. Mostly, the optimization of a single response is not possible without deteriorating the other responses. However, the application of the multi-objective optimization technique has been observed very helpful in the optimization of responses having conflicting nature [61]. In order to increase the CS of workpiece material, both SR and KW also need to be considered together.

3.4.1 Grey relational analysis

For multi-response optimization, GRA has been observed as the most effective technique. The technique can analyze

multiple parameters at the same time and minimize the deficiencies of primary statistical techniques during analysis. In this technique, response measure values are normalized in the decimals between 0 and 1. For this purpose, three distinct normalizing relations, (i) smaller the better, (ii) nominal the best, and (iii) larger the better (Eqs. (7), (8), and (9)), are used according to the nature of response measure [62]:

$$
\text{Larger the better } a_{ij} = \frac{\beta_{ij} - (\beta_{ij})_{min}}{(\beta_{ij})_{max} - (\beta_{ij})_{min}}
\tag{7}
$$

$$
\text{Nominal the best } \alpha_{ij} = 1 - \frac{|\beta_{ij} - \beta|}{(\beta_{ij})_{max} - \beta}
\tag{8}
$$

$$
\text{Smaller the better } \alpha_{ij} = \frac{(\beta_{ij})_{max} - \beta_{ij}}{(\beta_{ij})_{max} - (\beta_{ij})_{min}}
\tag{9}
$$

where α_{ij} is the ith normalized value of jth experiment, β_{ij} is the measured ith response value of jth experiment, and β is the desired/targeted response value. In the case of CS, larger the

better function is desirable, and smaller the better objective is preferred for both SR and KW.

To determine the relationship between optimum values and normalized values, grey relational coefficient has been practiced. Grey relational coefficient has been calculated using Eq. (10) given below:

$$\gamma_{ij} = \frac{(\Delta)_{min} + \xi(\Delta)_{max}}{\Delta_{ij} + \xi(\Delta)_{max}} \qquad (10)$$

where γ_{ij} is the grey relational coefficient of the ith normalized value of the jth experiment. ξ is the distinguishing coefficient, and its value is generally taken between 0 and 1. In this study, distinguishing coefficient ξ is taken at 0.5. Δ is the deviation from the desired/targeted value which is expressed as in Eqs. (11), (12), and (13) [63]:

$$\Delta_{max} = max_i max_j \left(y_i^o - y_{ij} \right) \qquad (11)$$

$$\Delta_{min} = min_i min_j \left(y_i^o - y_{ij} \right) \qquad (12)$$

$$\Delta_{ij} = \left(y_i^o - y_{ij} \right) \qquad (13)$$

The next step of GRA is the computation of GRG which is the weighting sum of all grey relational coefficients. GRG represents the relationship between input variables and all response measures simultaneously. It is presented in Eq. (14) below:

$$\delta_j = \frac{1}{n} \sum_{i=1}^{n} \gamma_{ij} \qquad (14)$$

where δ_j is the GRG of the jth experiment and n is the number of response measures (in current study n = 3). High GRG value represents the optimal set of input variables for all response measures simultaneously, and it is ranked as 1st. For the current study, Table 7 presents the grey relational coefficients, GRG, and their ranking for NT and CT wire electrodes.

Table 7 Multi-objective optimization using GRA for NT and CT wires

Exp. no.	Grey relational coefficient (NT wire)			Grey relational grade	Rank	Grey relational coefficient (CT wire)			Grey relational grade	Rank
	Cutting speed	Surface roughness	Kerf width			Cutting speed	Surface roughness	Kerf width		
1	0.339	0.689	0.403	0.477	25	0.339	0.619	0.390	0.450	26
2	0.571	0.467	0.335	0.458	28	0.556	0.425	0.334	0.438	29
3	0.398	0.588	0.644	0.543	14	0.400	0.518	0.824	0.581	4
4	1.000	0.333	0.381	0.571	6	1.000	0.333	0.398	0.577	5
5	0.357	0.672	0.412	0.480	24	0.362	0.603	0.406	0.457	25
6	0.403	0.536	0.459	0.466	27	0.403	0.562	0.448	0.471	24
7	0.389	0.722	0.528	0.547	12	0.377	1.000	0.504	0.627	2
8	*0.448*	*0.806*	*1.000*	*0.751*	*1*	*0.493*	*0.683*	*1.000*	*0.725*	*1*
9	0.337	0.778	0.421	0.512	21	0.333	0.672	0.438	0.481	22
10	0.574	0.381	0.350	0.435	30	0.533	0.353	0.399	0.429	30
11	0.353	0.758	0.700	0.604	2	0.349	0.645	0.811	0.602	3
12	0.709	0.491	0.409	0.536	15	0.698	0.483	0.426	0.536	9
13	0.384	1.000	0.392	0.592	3	0.397	0.804	0.381	0.528	13
14	0.495	0.695	0.487	0.559	10	0.518	0.588	0.475	0.527	14
15	0.435	0.842	0.448	0.575	5	0.450	0.687	0.434	0.524	17
16	0.574	0.544	0.583	0.567	7	0.600	0.483	0.564	0.549	6
17	0.333	0.918	0.427	0.560	9	0.336	0.853	0.415	0.534	10
18	0.543	0.487	0.333	0.455	29	0.535	0.475	0.333	0.448	27
19	0.358	0.777	0.500	0.545	13	0.360	0.734	0.478	0.524	16
20	0.775	0.430	0.381	0.529	18	0.743	0.422	0.372	0.513	19
21	0.363	0.711	0.384	0.486	23	0.362	0.600	0.357	0.440	28
22	0.459	0.470	0.491	0.473	26	0.458	0.424	0.536	0.473	23
23	0.393	0.796	0.509	0.566	8	0.391	0.663	0.578	0.544	8
24	0.524	0.549	0.667	0.580	4	0.521	0.485	0.640	0.549	7
25	0.437	0.674	0.491	0.534	17	0.418	0.644	0.509	0.523	18
26	0.455	0.711	0.479	0.548	11	0.430	0.676	0.496	0.534	11
27	0.430	0.641	0.467	0.513	20	0.408	0.614	0.484	0.502	20
28	0.435	0.674	0.496	0.535	16	0.422	0.644	0.513	0.526	15
29	0.441	0.619	0.514	0.525	19	0.426	0.630	0.531	0.529	12
30	0.432	0.637	0.444	0.504	22	0.418	0.610	0.462	0.497	21

Maximum GRG value (1) shows the optimum results at Exp No. 8 for both NT and CT wires

Fig. 13 Performance comparison of NT and CT wire electrodes
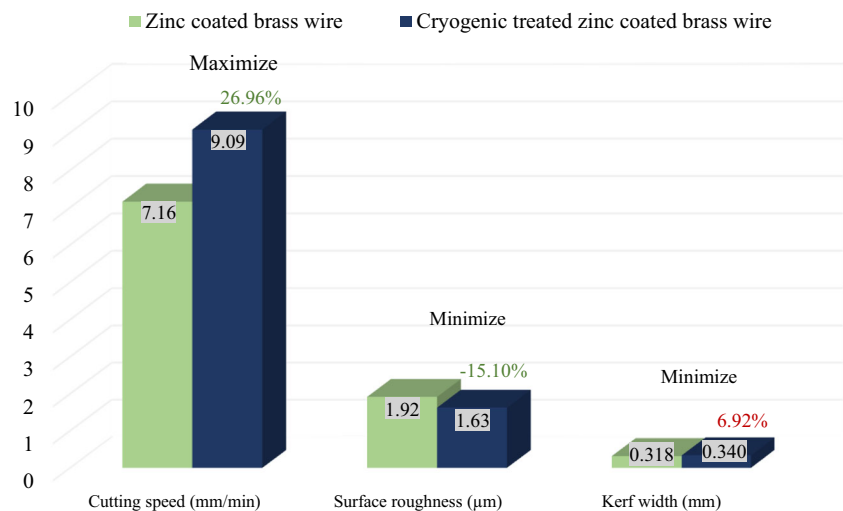
For both NT and CT wire electrodes, the highest GRG values 0.751 and 0.725 have been observed at exp. no. 08 respectively. Based on the highest GRG values, exp. no. 08 has been ranked as 1st among all values. This means that best values of CS, SR, and KW can be obtained simultaneously at $T_{ON} = 3$ μs, $F_R = 13$ m/min, $S_W = 11$ m/min, and $T_W = 10$ g by trading off responses to a limited extent.

3.5 Comparative performance analysis of wire electrodes

Although the response surface graphs have clearly revealed the remarkable performance of the CT wire for CS and SR, to further envision the efficiency of the CT wire electrode, optimum values of CS, SR, and KW have been compared. The percentage increase and decrease of response values of CT wire with respect to NT wire have been displayed in Fig. 13. As maximum CS values are desired, therefore, the comparison has been made at exp. no. 04 (provided in Table 5). CT wire yields 26.96 % high CS than NT wire. For Ra, the minimum values of both wires are compared at exp. no. 13. CT wire produces relatively 15.10 % less SR, so the percentage improvement is denoted by a negative sign in Fig. 13. CT wire on the other hand has generated 6.92% higher KW when its minimum values are analyzed at exp. no. 08. Based on the above discussion, it can be accomplished that the CT wire electrode is the best candidate for the machining of squeeze casted hybrid AMC.

4 Conclusion

This research aims to investigate the selection of potential wire electrode (wire type) and their effects on the machining performance of the squeeze casted $Al2024/Al_2O_3/W$ hybrid composite in the WEDM process. Based on experimental

consequences and findings from their respective discussion, some salient conclusions are figured out:

- The hybrid composite fabricated with the squeeze casting process presents significant mechanical properties and uniform dispersion of particles throughout the metal matrix.
- Cryogenic treatment declined the electrical conductivity of molybdenum wire and improved UTS to a limited extent. On the other hand, the electrical conductivity of zinc-coated brass wire was significantly escalated by 24.8% with cryogenic treatment which depicted the CT brass wire as the potential candidate for machining of squeeze casted $Al2024/Al_2O_3/W$.
- ANOVA showed that T_{ON} was the most significant input variable for the CS, SR, and KW, while F_R, T_W, and S_W were the subsequent substantial input variables for both wires.
- Surface morphology analysis of machined surfaces of AMC characterized that high energy parameters with NT wire generate a surface with a high concentration of micro-voids, globules, and deep and larger craters which were reduced by practicing low energy parameters with CT wire.
- SEM analysis revealed that there exists a high concentration of micro-voids and deep craters on the surface of NT wire while shallow craters and a quite smooth surface have been observed in CT wire after machining.
- Multi-objective optimization based on GRA presented $T_{ON} = 3$ μs, $F_R = 13$ m/min, $S_W = 11$ m/min, and $T_W = 10$ g as an optimal set of input variables to achieve 75.1% and 72.5% overall results with NT and CT wire respectively by trading off up to a limited extent.
- Comparative analysis of the optimum values of performance measures of wire electrode divulged that CT wire electrode offers 26.96% and 15.10% superior results for

CS and SR respectively while 6.92% deprived results for KW than NT wire.

This research proposed a suitable wire electrode for the squeeze casted hybrid AMC in the WEDM process, which can be helpful for the practitioners in the machining of such type of material on the industrial scale. Future research can be conducted to analyze the effects of suggested wire type on recast layer thickness, microhardness, and infusion of wire material on the workpiece surface. That study will provide an in-depth analysis of the surface morphology of the workpiece machined with the recommended wire electrode.

Nomenclature WEDM, Wire electric discharge machining; AMC, Aluminum matrix composite; T_{ON}, Pulse duration; F_R, Wire feed rate; S_W, Wire runoff speed; T_W, Wire tension; T_{OFF}, Pulse off time; CS, Cutting speed; SR, Surface roughness; KW, Kerf width; I, Discharge current; V, Gap voltage; SEM, Scanning electron microscope; CT wire, Cryogenic treated zinc-coated brass wire; NT wire, Non-cryogenic treated zinc-coated brass wire; UTS, Ultimate tensile strength; RSM, Response surface methodology; ANOVA, Analysis of variance; GRA, Grey relational analysis; GRG, Grey relational grade

Author contribution Conceptualization, Methodology, Writing original draft: Muhammad Huzaifa Raza. Conceptualization, Data curation, Investigation and visualization: Muhammad Asad Ali. Resources, Investigation and Experimentation: Waseem Tahir. Supervision, Review and editing: Ray Y. Zhong. Review and editing: Nadeem Ahmad Mufti, Naveed Ahmad.

Declarations

Ethics approval Not applicable.

Consent to Participate Not applicable.

Consent for Publication Not applicable.

Competing interests The authors declare no competing interests.

References

1. Pramanik A (2016) Effects of reinforcement on wear resistance of aluminum matrix composites. Trans Nonferrous Metals Soc China 26(2):348–358
2. Dinaharan I et al (2016) Microstructure and wear characterization of aluminum matrix composites reinforced with industrial waste fly ash particulates synthesized by friction stir processing. Mater Charact 118:149–158
3. Lu T et al (2020) Microstructure, mechanical properties and machinability of particulate reinforced Al matrix composites: a comparative study between SiC particles and high-entropy alloy particles. Journal of Materials Research and Technology 9(6): 13646–13660
4. Zhang C et al (2017) Enhanced tensile properties of Al matrix composites reinforced with β-Si3N4 whiskers. Compos A: Appl Sci Manuf 102:145–153
5. Gebler, M., A.J.S. Uiterkamp, and C.J.E.P. Visser (2014) A global sustainability perspective on 3D printing technologies. 74: p. 158-167.
6. Idrisi AH, Mourad A-HI (2019) Conventional stir casting versus ultrasonic assisted stir casting process: mechanical and physical characteristics of AMCs. J Alloys Compd 805:502–508
7. Nemtajela N, Mbohwa C (2017) Relationship between inventory management and uncertain demand for fast moving consumer goods organisations. Procedia Manufacturing 8:699–706
8. Sarfraz MH et al (2019) Multi-response parametric optimization of squeeze casting process for fabricating Al 6061-SiC composite. Int J Adv Manuf Technol 102(1):759–773
9. Liao Z et al (2019) State-of-the-art of surface integrity in machining of metal matrix composites. Int J Mach Tools Manuf 143:63–91
10. Senthil P, Selvaraj T, Sivaprasad K (2013) Influence of turning parameters on the machinability of homogenized Al–Cu/TiB 2 in situ metal matrix composites. Int J Adv Manuf Technol 67(5-8): 1589–1596
11. Bejjani R et al (2016) Chip formation and microstructure evolution in the adiabatic shear band when machining titanium metal matrix composites. Int J Mach Tools Manuf 109:137–146
12. Pugazhenthi A et al (2018) Turning characteristics of in situ formed TiB2 ceramic particulate reinforced AA7075 aluminum matrix composites using polycrystalline diamond cutting tool. Measurement 121:39–46
13. Dandekar CR, Shin YC (2012) Modeling of machining of composite materials: a review. Int J Mach Tools Manuf 57:102–121
14. Nicholls CJ et al (2017) Review of machining metal matrix composites. Int J Adv Manuf Technol 90(9-12):2429–2441
15. Raju R et al (2018) Optimization of process parameters in electrical discharge machining of haste alloy C276 using Taguchi's method. Materials Today: Proceedings 5(6, Part 2):14432–14439
16. Reolon LW et al (2019) WEDM performance and surface integrity of Inconel alloy IN718 with coated and uncoated wires. Int J Adv Manuf Technol 100(5-8):1981–1991
17. Tahir W, Jahanzaib M (2019) Multi-objective optimization of WEDM using cold treated brass wire for HSLA hardened steel. J Braz Soc Mech Sci Eng 41(11):525
18. Gong Y et al (2017) Experimental study on surface integrity of Ti-6Al-4V machined by LS-WEDM. Int J Adv Manuf Technol 88(1): 197–207
19. Paswan K, Pramanik A, Chattopadhyaya S (2020) Machining performance of Inconel 718 using graphene nanofluid in EDM. Mater Manuf Process 35(1):33–42
20. Muniappan A et al (2019) Optimization of WEDM process parameters for cutting speed using Taguchi technique. Materials Today: Proceedings 18:332–341
21. Satishkumar D, Kanthababu M (2014) Optimization of Wedm parameters for surface roughness on hybrid Mmcs. Adv Compos Lett 23(3):096369351402300303
22. Ugrasen G et al (2018) Estimation of machining performances using MRA and GMDH in wire EDM of Al2024 based hybrid MMC. Materials Today: Proceedings 5(1, Part 3):3084–3092
23. Nag A et al (2018) Surface integrity analysis of wire-EDM on in-situ hybrid composite A359/Al2O3/B4C. Materials Today: Proceedings 5(11, Part 3):24632–24641
24. Kumar SS et al (2015) Parametric optimization of wire electrical discharge machining on aluminium based composites through grey relational analysis. J Manuf Process 20:33–39
25. Udaya Prakash J et al (2018) Optimization of wire EDM process parameters for machining hybrid composites (356/B4C/Fly Ash)

using Taguchi technique. Materials Today: Proceedings 5(2, Part 2):7275–7283

26. Lal S et al (2014) Wire electrical discharge machining of AA7075/SiC/Al2O3 hybrid composite fabricated by inert gas-assisted electromagnetic stir-casting process. J Braz Soc Mech Sci Eng 36(2):335–346

27. Ishfaq, K., et al. (2020) Optimization of WEDM for precise machining of novel developed Al6061-7.5% SiC squeeze-casted composite. The International Journal of Advanced Manufacturing Technology.

28. Tahir W, Jahanzaib M, Raza A (2019) Effect of process parameters on cutting speed of wire EDM process in machining HSLA steel with cryogenic treated brass wire. Advances in Production Engineering & Management 14(2):143–152

29. Goyal A (2017) Investigation of material removal rate and surface roughness during wire electrical discharge machining (WEDM) of Inconel 625 super alloy by cryogenic treated tool electrode. Journal of King Saud University-Science 29(4):528–535

30. Özbek NA et al (2014) Investigation of the effects of cryogenic treatment applied at different holding times to cemented carbide inserts on tool wear. Int J Mach Tools Manuf 86:34–43

31. Yao Y, Zhou Y (2018) Effects of deep cryogenic treatment on wear resistance and structure of GB 35CrMoV steel. Metals 8(7):502

32. Senthilkumar D, Rajendran I (2012) Optimization of deep cryogenic treatment to reduce wear loss of 4140 steel. Mater Manuf Process 27(5):567–572

33. Seah K, Rahman M, Yong K (2003) Performance evaluation of cryogenically treated tungsten carbide cutting tool inserts. Proc Inst Mech Eng B J Eng Manuf 217(1):29–43

34. Kapoor J, Khamba JS, Singh S (2012) Effect of shallow cryogenic treated brass wire electrode on workpiece surface roughness in wire-EDM. International Journal of Materials Engineering Innovation 3(3-4):190–203

35. Kapoor J, Singh S, Khamba JS (2012) Effect of cryogenic treated brass wire electrode on material removal rate in wire electrical discharge machining. Proc Inst Mech Eng C J Mech Eng Sci 226(11):2750–2758

36. Nayak BB, Mahapatra SS (2016) Optimization of WEDM process parameters using deep cryo-treated Inconel 718 as work material. Engineering Science and Technology, an International Journal 19(1):161–170

37. Raza MH et al (2018) Investigating the effects of different electrodes on Al6061-SiC-7.5 wt% during electric discharge machining. Int J Adv Manuf Technol 99(9):3017–3034

38. Kapoor J, Singh S, J.S.J.P.o.t.I.o.M.E. Khamba (2012) Effect of cryogenic treated brass wire electrode on material removal rate in wire electrical discharge machining. Part C: Journal of Mechanical Engineering Science 226(11):2750–2758

39. Beutel A-L, Minner S (2012) Safety stock planning under causal demand forecasting. Int J Prod Econ 140(2):637–645

40. Murr, L. and S.J.C.M.P. Gaytan (2014) Advances in additive manufacturing and tooling, Elsevier. p. 135-161.

41. Spoerk, M., C. Holzer, and J. Gonzalez-Gutierrez (2020) Material extrusion-based additive manufacturing of polypropylene: a review on how to improve dimensional inaccuracy and warpage. 137(12): p. 48545.

42. de Kok T et al (2018) A typology and literature review on stochastic multi-echelon inventory models. Eur J Oper Res 269(3):955–983

43. Patel GC, Shettigar MAK, Parappagoudar MB (2018) A systematic approach to model and optimize wear behaviour of castings produced by squeeze casting process. J Manuf Process 32:199–212

44. Luo, R.C., C.H. Hsu, and Y.C. Wen (2020) Multi-model fusion on real-time drowsiness detection for telemetric robotics tracking applications. in 2020 International Conference on Advanced Robotics and Intelligent Systems (ARIS).

45. Montgomery, D.C. (2017) Design and analysis of experiments: John wiley & sons.

46. Ali MA et al (2018) Evaluating the effects of as-casted and aged overcasting of Al-Al joints. Int J Adv Manuf Technol 96(1):1377–1392

47. Kavimani V, Prakash KS, Thankachan T (2019) Multi-objective optimization in WEDM process of graphene–SiC-magnesium composite through hybrid techniques. Measurement 145:335–349

48. Gopal PM, Prakash KS, Jayaraj S (2018) WEDM of Mg/CRT/BN composites: effect of materials and machining parameters. Mater Manuf Process 33(1):77–84

49. Rajmohan K, Kumar AS (2017) Experimental investigation and prediction of optimum process parameters of micro-wire-cut EDM of 2205 DSS. Int J Adv Manuf Technol 93(1-4):187–201

50. Habib S, Okada A (2016) Experimental investigation on wire vibration during fine wire electrical discharge machining process. Int J Adv Manuf Technol 84(9):2265–2276

51. Chen Z et al (2017) Theoretical and experimental study of magnetic-assisted finish cutting ferromagnetic material in WEDM. Int J Mach Tools Manuf 123:36–47

52. Manjaiah M et al (2015) Effect of electrode material in wire electro discharge machining characteristics of Ti50Ni50−xCux shape memory alloy. Precis Eng 41:68–77

53. Habib S (2017) Optimization of machining parameters and wire vibration in wire electrical discharge machining process. Mechanics of Advanced Materials and Modern Processes 3(1):3

54. Habib S, Okada A (2016) Study on the movement of wire electrode during fine wire electrical discharge machining process. J Mater Process Technol 227:147–152

55. Raza, M.H., et al. (2019) Grain selection and crystal orientation in single-crystal casting: state of the art. 54(2): p. 1800177.

56. Tahir, W., et al. (2019) Surface morphology evaluation of hardened HSLA steel using cryogenic-treated brass wire in WEDM process. 104(9-12): p. 4445-4455.

57. Krishnaiah, K. and P. Shahabudeen(2012) Applied design of experiments and Taguchi methods: PHI Learning Pvt. Ltd.

58. Raza MH et al (2019) Modeling of the mechanical properties of directionally solidified Al-4.3% Cu alloy using response surface methodology. Int J Adv Manuf Technol:1–13

59. Ali MA et al (2020) Mechanical characterization of aged AA2026-AA2026 overcast joints fabricated by squeeze casting. Int J Adv Manuf Technol:1–21

60. Leung WK, Raza MH, Zhong RY (2021) Optimization of support structure in multi-articulated joints of non-assembly mechanisms. Procedia CIRP 100:726–731

61. Yuan J et al (2008) Reliable multi-objective optimization of high-speed WEDM process based on Gaussian process regression. Int J Mach Tools Manuf 48(1):47–60

62. Ishfaq K et al (2019) Evaluating material's interaction in wire electrical discharge machining of stainless steel (304) for simultaneous optimization of conflicting responses. Materials 12(12):1940

63. Wojciechowski S et al (2018) Application of signal to noise ratio and grey relational analysis to minimize forces and vibrations during precise ball end milling. Precis Eng 51:582–596